Research Square

Preprints are preliminary reports that have not undergone peer review.
They should not be considered conclusive, used to inform clinical practice,
or referenced by the media as validated information.

Microstructural Evolution, Surface Integrity and Fatigue Resistance of Laser-Cut Strenx 700cr Steel

João Vitor Miszewski

212236@upf.br

Universidade de Passo Fundo

William Haupt

Universidade de Passo Fundo

Diogo Teixeira

Universidade de Passo Fundo

Cleiton Gnich

Universidade de Passo Fundo

Matheus Giongo Pavan

Universidade de Passo Fundo

André Amaral dos Santos

Universidade de Passo Fundo

Research Article

Keywords: Laser cutting, High strength low alloy steel, Microstructure, Fatigue, Surface roughness, Strenx 700CR

Posted Date: June 23rd, 2026

DOI: https://doi.org/10.21203/rs.3.rs-10020784/v1

License: This work is licensed under a Creative Commons Attribution 4.0 International License.
Read Full License

Additional Declarations: No competing interests reported.

MICROSTRUCTURAL EVOLUTION, SURFACE INTEGRITY AND FATIGUE RESISTANCE OF LASER-CUT STRENX 700CR STEEL

João Vitor Miszewski[1,2], William Haupt[1], Diogo Teixeira[1], Cleiton Gnich[1], Matheus Giongo Pavan[1], André Amaral dos Santos[1]

ABSTRACT

High-strength low-alloy steels are widely used in structural applications due to their high strength-to-weight ratio. However, the thermal effects of laser cutting may modify the cut edge, altering its microstructure, surface integrity, and mechanical performance. This study evaluated the influence of laser power and assist gas on the roughness, microhardness, microstructure, thermally modified zones, and fatigue resistance of 2 mm thick Strenx 700CR steel. Four experimental combinations involving laser powers of 2500 and 3000 W and the assist gases oxygen and nitrogen were investigated. The samples were characterized by metallographic analyses, scanning electron microscopy, Vickers microhardness, surface roughness measurements, and axial fatigue testing. The results demonstrated that the areas of the cast zone (CZ) and heat affected zone (HAZ) increased with laser power and were larger under oxygen-associated conditions, with the assist gas condition being the dominant factor, contributing 79.40% and 63.15% to the variation of the CZ and HAZ areas, respectively. The cast zone exhibited a higher fraction of bainite and constituents compatible with martensite, resulting in microhardness values higher than those of the base material, whereas the HAZ exhibited softening. The Ra and Rz roughness parameters were higher at the cut exit, with increases ranging from 184.01% to 430.45%, and the measurement position was the predominant factor. The retention of the modified regions reduced fatigue life by up to 83%, with crack nucleation occurring predominantly at the cut exit. However, condition EC2 exhibited superior performance under a stress level of 539 MPa, which was associated with its lower Rz value.

Keywords: Laser cutting • High strength low alloy steel • Microstructure • Fatigue • Surface roughness • Strenx 700CR

1. INTRODUCTION

The reduction of structural mass has become a strategic approach to improve energy efficiency, reduce pollutant emissions, and enhance the performance of components in several fields of mechanical engineering (1-2). In this context, high strength low alloy (HSLA) steels have been widely employed due to their high strength-to-weight ratio, with applications in truck bodies, railway wagons, automotive chassis, and aircraft structures (3-5). In parallel with material selection, manufacturing processes also play a fundamental role in the final performance of components. Laser beam cutting stands out due to its high dimensional precision, flexibility in producing complex geometries, and potential to optimize material utilization through strategies such as nesting (6-8).

[1] Postgraduate Program in Design and Manufacturing Processes, Department of Mechanical Engineering, University of Passo Fundo, Passo Fundo, Rio Grande do Sul, Brazil.

[2] Cavaletti S/A – Professional Chairs, Erechim, Rio Grande do Sul, Brazil.

However, the thermal nature of the process may compromise the surface integrity of the cut edges, directly influencing the mechanical behavior during service. Laser–material interaction is governed by the flow dynamics of molten material at the cutting front, with hump formation being associated with this flow behavior. Fluctuations in the thickness of the liquid film, combined with the interaction with the assist gas, may result in flow instabilities, manifesting as periodic oscillations of the cutting front (9-10).

In this context, HSLA steels such as Strenx 700, due to their high mechanical strength and toughness associated with a refined microstructure obtained through thermomechanically controlled processing, as well as the presence of precipitates of microalloying elements such as Nb, Ti, and V, become susceptible to the thermal variations imposed by laser cutting (3, 11-12).

The laser cutting process induces changes in the surface integrity of the material, which are critical to its performance and durability in service and may compromise properties such as fatigue resistance, creep, corrosion, and wear. These changes manifest through the formation of surface defects and modifications in mechanical properties, topography, and chemical composition (13-15).

In this context, instabilities in molten material flow result in the formation of striations, which are responsible for defining the morphology and roughness of the obtained surface (15). Furthermore, the increase in molten material volume, frequently associated with combinations of high power and low cutting speed, tends to intensify this behavior, resulting in more irregular surfaces with higher roughness (7).

Burr formation and increased roughness act as stress concentrators, favoring crack nucleation and consequently reducing the fatigue life of components. Additionally, the greater the presence of cutting striations, the lower the fatigue resistance tends to be, due to crack nucleation originating from these surface discontinuities (16-19).

In addition to the effects on surface integrity, the laser cutting process directly influences the material microstructure. For example, in S355J2 structural steel, changes from a microstructure predominantly composed of ferrite and pearlite to a ferrite and austenite combination have been observed (20). Furthermore, laser cutting of Strenx steels introduces residual stresses and work hardening, leading to an increase between 14% and 30% in the surface hardness of S700 alloy (21).

In general, the final surface quality, frequently evaluated by roughness, is strongly influenced by cutting speed, since higher values reduce heat input and consequently decrease the width of the heat affected zone (HAZ) and the size of striations. In contrast, roughness tends to increase with laser power, as excessive thermal energy may promote uncontrolled melting, increasing both roughness and kerf width. In this regard, laser power may account for more than 54% of the roughness variation in steels such as Strenx 900. Thus, to minimize roughness and preserve microstructural integrity, the combination of lower laser power and higher cutting speed is recommended, provided that assist gas pressures are sufficient to ensure efficient removal of molten material (6-7).

Additionally, assist gases also exert significant influence on cut quality. Oxygen, for example, is widely used in cutting thick ferrous alloys due to its exothermic reaction, which may provide between 55% and 70% of the total process energy, enabling higher cutting speeds. However, this reaction tends to increase the HAZ and promote surfaces with higher roughness and greater burr formation when compared with inert gases. In contrast, nitrogen is preferred when improved surface quality and lower HAZ are desired, since it protects the edge against oxidation reactions at high temperatures, although it requires higher laser powers (6-7).

Despite the industrial relevance of Strenx steels, limitations still exist in the literature regarding the integrated understanding of the effects of laser power and assist gases on the surface integrity and fatigue performance of Strenx 700CR. Furthermore, studies simultaneously relating microstructural characteristics, mechanical properties, and operational conditions remain scarce, especially from an applied perspective. Therefore, the present work aims to evaluate the influence of laser cutting parameters on roughness, microhardness, heat affected zone, and fatigue resistance of Strenx 700CR steel.

2. MATERIALS AND METHODS

2.1. Materials

The material used in this study was the high strength structural steel Strenx 700CR, manufactured by Swedish Steel Company and supplied as rolled sheets with a thickness of 2 mm. Initially, the chemical composition of the base material was determined by optical emission spectrometry using an Oxford Foundry-Master X-Line spectrometer. The obtained results are presented in Table 1. Additionally, the mechanical properties of the material, including yield strength, tensile strength, and elongation, are presented in Table 2.

Table 1 Chemical composition of Strenx 700CR steel

Material	Elements (wt.%)						
	C	Si	Mn	P	S	Al	Nb + Ti
Strenx 700CR	0.15	0.14	1.50	0.010	0.010	0.17	0.014

Table 2 Mechanical properties of Strenx 700CR steel

Material	Yield strength (MPa)	Tensile strength (MPa)	Elongation (%)
Strenx 700CR	973 ± 50.22	1077 ± 20.88	9.96 ± 0.35

2.2. Laser Cutting Procedures

The analyzed samples were sectioned by fiber laser cutting using an industrial ULF-3015 cutting machine manufactured by Okada, shown in Fig. 1. Two assist gases were used, oxygen and nitrogen, both with a purity of 99.99%, at pressures of 3 bar and 15 bar and cutting speeds of 4.2 m/min and 8 m/min, respectively, combined with two laser power levels, 2500 W and 3000 W. Additionally, the lens focal position, nozzle diameter, and laser beam diameter were kept constant at 2.0 mm, 1.2 mm, and 1.2 mm, respectively. The experimental combinations are described in Table 3.

Fig. 1 ULF-3015 fiber laser cutting machine manufactured by Okada



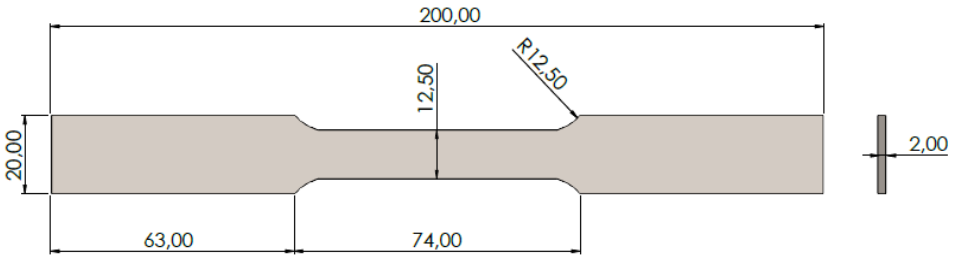
Table 3 Experimental conditions applied

Experimental condition	Laser power (W)	Cutting speed (m/min)	Assist gas	Gas pressure (bar)
EC1	2500	4.2	Oxygen	3
EC2	3000	4.2	Oxygen	3
EC3	2500	8	Nitrogen	15
EC4	3000	8	Nitrogen	15

2.3. Tensile Test

The tensile tests were carried out in accordance with ASTM E8M using standardized specimens with the geometry shown in Fig. 2. The tests were conducted on a UPM200 universal testing machine manufactured by Shenk. Three specimens were tested under uniaxial loading at a strain rate of 0.5 mm/min. It should be noted that, in order to minimize the influence of the heat affected zone on the results, these samples were produced while maintaining an allowance layer during laser cutting, which was subsequently removed by machining.

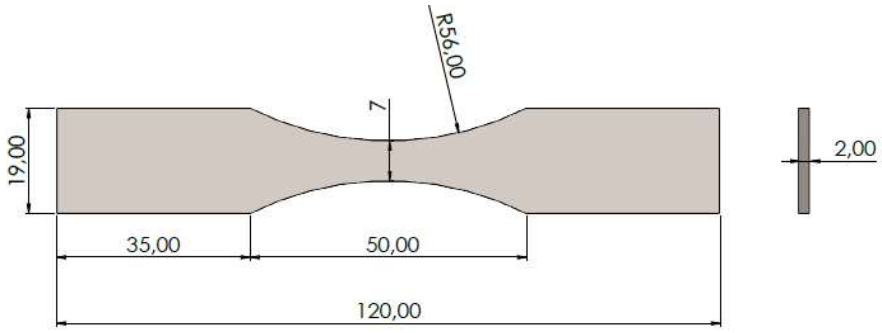
Fig. 2 Dimensions of the tensile test specimen (ASTM E8M)



2.4. Fatigue Test

The fatigue tests were conducted in accordance with ASTM E466-21 using three specimens for each sampling condition, following the geometry shown in Fig. 3. The tests were performed on a Shimadzu servo-hydraulic testing machine, model EHF-EV101. The maximum loads applied under tensile cyclic loading were defined as 50% and 70% of the ultimate tensile strength previously determined for Strenx 700CR in the condition without the presence of the heat affected zone produced by laser cutting, corresponding to 7546 N and 10556 N, respectively. The adopted stress ratio was 0.1 and the test frequency was 3 Hz.

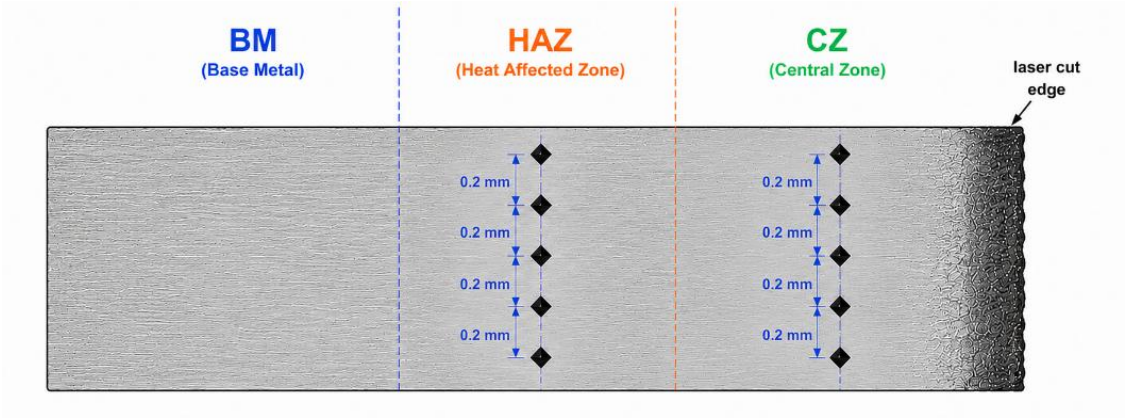
Fig. 3 Dimensions of the fatigue test specimen (ASTM E466-21)



2.5. Vickers Microhardness

The microhardness measurements were performed in accordance with ASTM E384. Ten measurements were carried out along the central line of the specimen cross section, starting at 0.2 mm from the edge and ending at 2.00 mm from this reference point, thus maintaining an indentation spacing of 0.2 mm, as illustrated in Fig. 4. The Vickers scale was employed using a load of 0.3 kgf applied for 15 seconds. The equipment used was a Shimadzu HMW-G 20ST microhardness tester.

Fig. 4 Microhardness measurement procedure

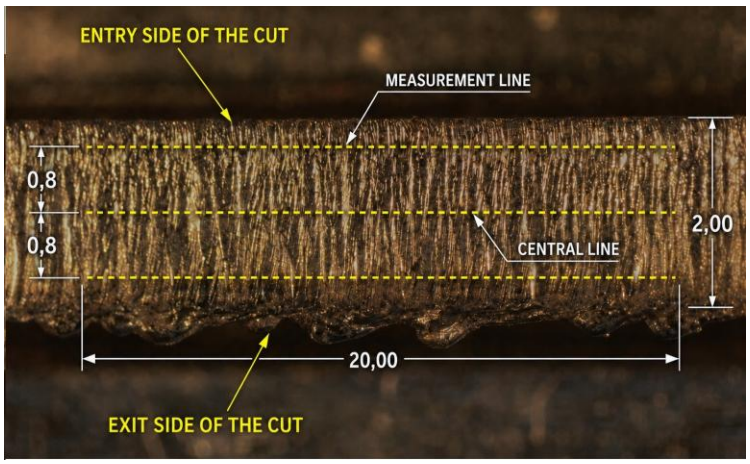


2.6. Surface Roughness

The surface roughness of the cut regions was evaluated through measurements performed using a Mitutoyo SJ-410 roughness tester. The roughness parameters Ra and Rz were determined directly on the cut

surface of the specimens, following the criteria established by ISO 4287 and ISO 4288. Three specimens from each experimental condition were evaluated, with five measurements carried out at both the cut entry and cut exit regions, approximately 0.8 mm from the center of the specimen thickness, as illustrated in Fig. 5. Based on these data, the average Ra and Rz values were calculated for each experimental combination.

Fig. 5 Surface roughness measurement procedure



2.7. Metallography and Fractography

The samples intended for metallographic analysis were mounted in bakelite and subsequently subjected to manual grinding using silicon carbide abrasive papers lubricated with water, following the grit sequence of 150, 220, 400, 600, 1000, and 2000 mesh. After grinding, the samples were mechanically polished using a 1.0 μm alumina suspension. Chemical etching was then performed using Nital reagent, with the concentration and etching time varying according to the type of analysis performed.

For optical micrographs, 2% Nital was used for 15 seconds. For optical macrographs, a 10% Nital solution was applied for 10 seconds. For microstructural analyses performed by scanning electron microscopy (SEM), 2% Nital was used for 20 seconds. Macroscopic and microscopic analyses by optical microscopy were carried out using an Olympus SZ61 stereomicroscope and an Olympus BX51M optical microscope, respectively. SEM analyses, both metallographic and fractographic, were performed using a Vega LM3 scanning electron microscope manufactured by Tescan, operating in secondary electron mode.

3. RESULTS AND DISCUSSION

3.1. Cross Section Analysis of the Cut Region

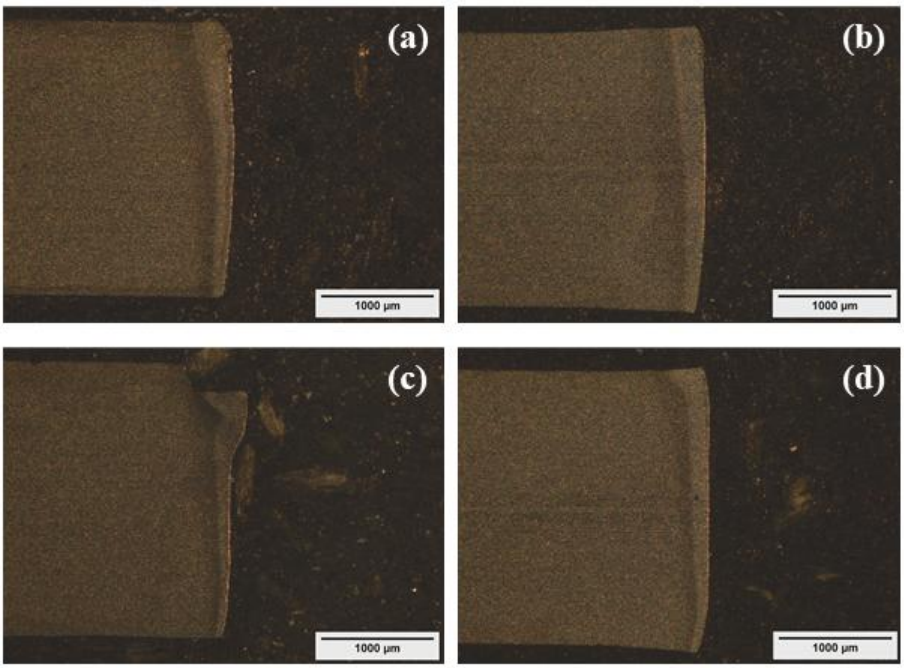
The heat deposited during laser cutting resulted in the formation of thermally affected regions along the cut edge, as shown in Fig. 6. These regions were subdivided into the cast zone (CZ), located immediately adjacent to the cut surface, and the heat affected zone (HAZ), situated between the cast zone and the base material. Analysis of the macrographs revealed that the width of both regions progressively decreased with

increasing distance from the cut entry surface. Therefore, the entry region was more intensely affected by the thermal cycle imposed by the laser beam than the exit region (7).

This behavior is associated with the non-uniform energy distribution along the material thickness during laser cutting. In the entry region, the higher energy density promotes elevated temperatures and greater lateral thermal diffusion. As the beam penetrates the material, part of its energy is progressively attenuated, while the flow of molten material and heat extraction by the assist gas contribute to reducing the extent of the affected region (7).

The quantitative analysis of the areas occupied by the cast zone and the heat affected zone is presented in Fig. 7. For both zones, the oxygen-assisted conditions resulted in larger areas than those obtained using nitrogen. Furthermore, for a given assist gas, increasing the laser power from 2500 W to 3000 W promoted an increase in the areas occupied by the thermally affected regions. This behavior indicates that both laser power and the assist gas condition influenced the thermal extent of the cut edge.

Fig. 6 Macrographs of the cross section of laser-cut specimens: (a) EC1; (b) EC2; (c) EC3; and (d) EC4



The greater extent of the affected regions under oxygen-assisted conditions is associated with the additional heat generated by the exothermic reaction between oxygen and the molten metal, which increases the effective heat input during cutting. In contrast, nitrogen acts as an inert assist gas, limiting oxidation reactions and reducing the thermal effect on the cut edge (7). This behavior is also consistent with the main effect plots presented in Fig. 8, in which a tendency toward reduced areas of both the cast zone and the heat affected zone can be observed under nitrogen-associated conditions.

The results of the ANOVA analysis for both zones statistically confirmed the trends observed in Fig. 8. For both the heat affected zone and the cast zone, the condition associated with the employed assist gas was the dominant factor controlling the affected areas, contributing 63.15% and 79.40%, respectively. The second greatest source of contribution was laser power, with contributions of 12.92% and 18.12%. However, the

interaction between these factors did not present an effective contribution for either region, yielding p = 0.965 for the heat affected zone and p = 0.858 for the cast zone.

It should be emphasized that cutting speed and gas pressure were not kept constant between the oxygen and nitrogen conditions. Therefore, the effect attributed to the assist gas should be interpreted as the result of the combined influence of gas type, cutting speed, and gas pressure. Even considering this limitation, the results indicate that the oxygen-associated cutting condition promoted a greater extent of the thermally affected regions, whereas the nitrogen-associated condition reduced the areas of both the heat affected zone and the cast zone.

Fig. 7 Area occupied by the cast zone and the heat affected zone for each experimental condition

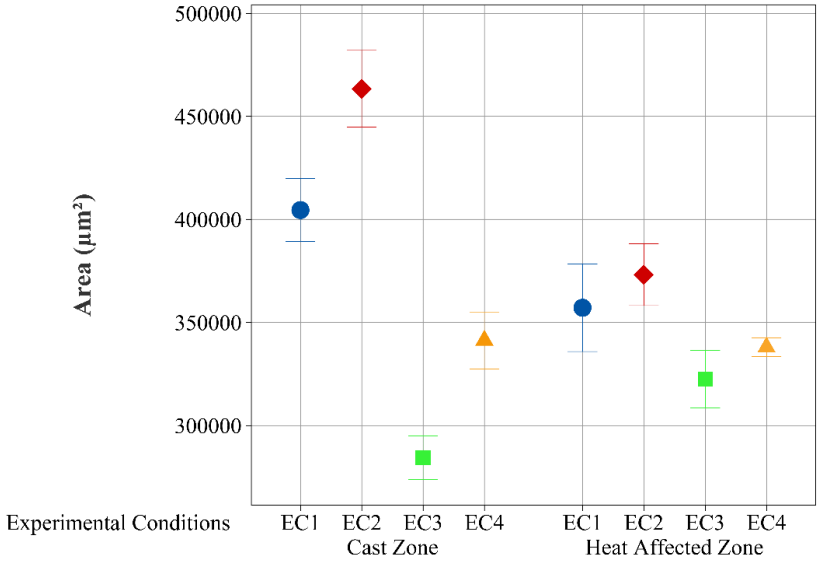
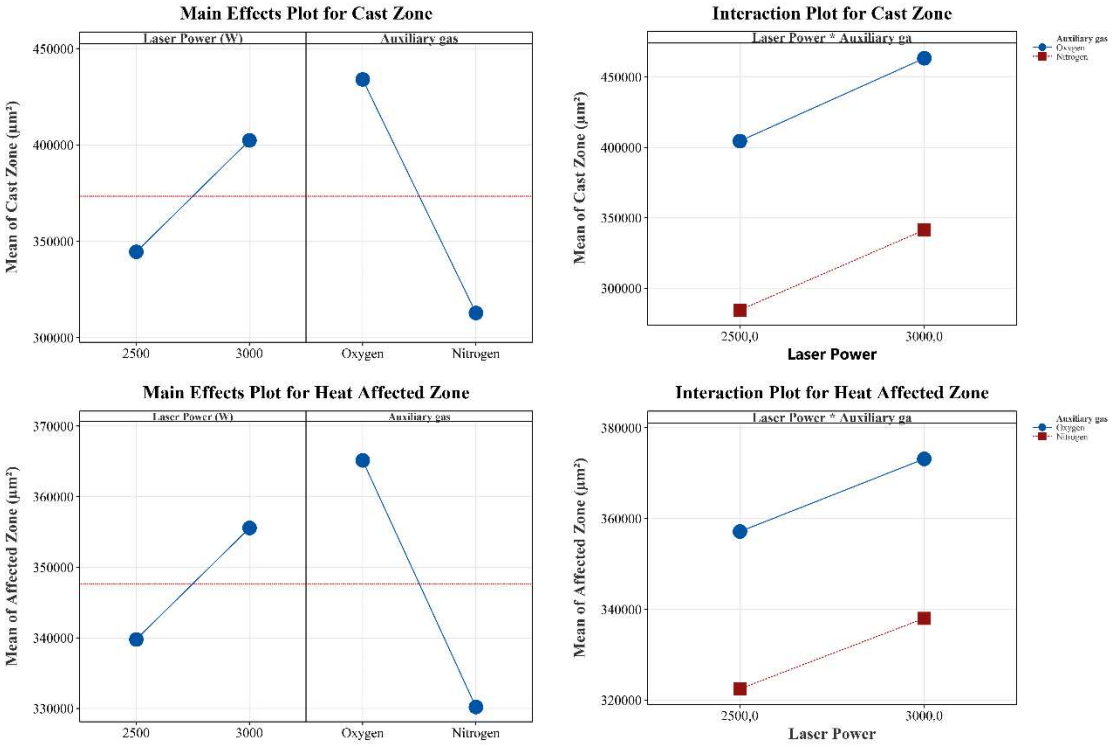


Fig. 8 Main effect and interaction plots for the area of the cast zone and the heat affected zone

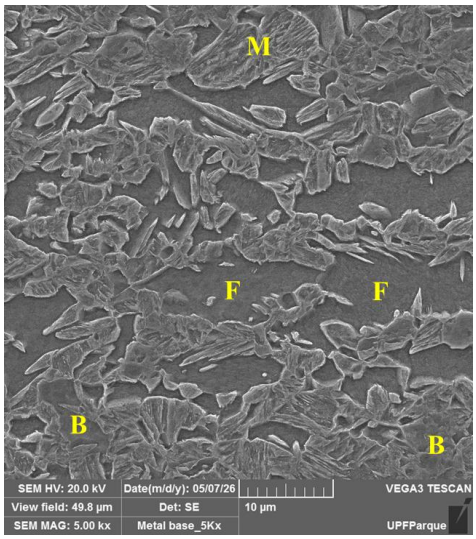


3.2. Microstructure

As a result of the thermomechanically controlled processing employed in the manufacture of Strenx 700, the base material exhibits a ferritic-bainitic matrix as its main constituent. In addition, the microalloying elements present in the steel, such as Nb, Ti, and V, contribute to microstructural refinement through the formation of precipitates dispersed throughout the matrix (3; 22). Fig. 9 presents the microstructure of the base material, without the influence of laser cutting. From this analysis, the predominant presence of ferrite (F) and lath bainite (B), as well as regions compatible with martensite (M), can be identified, in agreement with the constituents described by Bukovská *et al*. (2022) [3] and Trško *et al*. (2020) [22].

As previously mentioned, the heat input during the laser cutting process promoted the formation of a thermally affected region subdivided into a cast zone and a heat affected zone. In the optical microscopy images, the cast zone exhibits a lighter appearance, whereas the heat affected zone can be distinguished by its darker coloration relative to the adjacent material, as observed in Fig. 10. Furthermore, the cast zone presents a lower relative presence of ferrite, while this constituent progressively occupies a larger fraction within the heat affected zone and the base material.

Fig. 9 Microstructure of Strenx 700CR in its original condition



A similar microstructural behavior was observed by Ilin, Krasnoperova, and Sirotkin (2019) [23] in S700MC steel, who attributed the darker appearance of the affected region to bainite tempering. This phenomenon is associated with the softening of the heat affected zone in several ultra-high-strength steels. In Docol PHS CR 2000, for example, softening occurs due to the formation of tempered martensite and ferrite, with the maximum hardness loss located at the boundary between the intercritical and subcritical zones (24). In S960 and S1100 alloys, the reduction in hardness is caused by the nucleation of ferrite and granular bainite (25).

Analysis of the heat affected zone and cast zone by scanning electron microscopy, presented in Figs. 11 to 14, revealed that the different experimental conditions produced similar microstructures with respect to the formed constituents. In general, the heat affected zone exhibited greater similarity to the base material, being predominantly composed of ferrite and lath bainite, together with localized regions compatible with martensite. In turn, the cast zone exhibited a greater predominance of bainite and constituents with morphology compatible with martensite, in addition to a lower relative ferrite content. This behavior is attributed to melting followed by

rapid solidification in the region close to the cut surface, favoring the formation of harder constituents. Among the analyzed conditions, EC3 enabled a clearer observation of the transition between the cast zone and the heat affected zone, as shown in Fig. 13 (a), as well as the reduction in ferrite fraction within the cast zone, as presented in Fig. 13 (b).

Fig. 10 Microstructure of the heat affected region for the experimental conditions: (a) EC1; (b) EC2; (c) EC3; and (d) EC4 obtained by optical microscopy

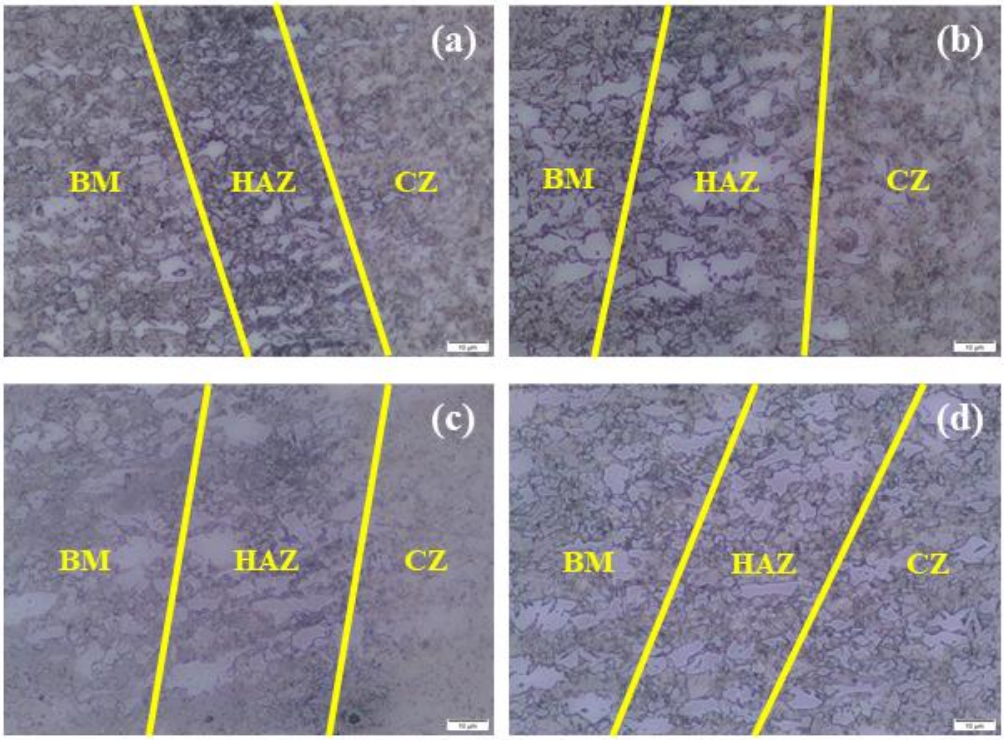
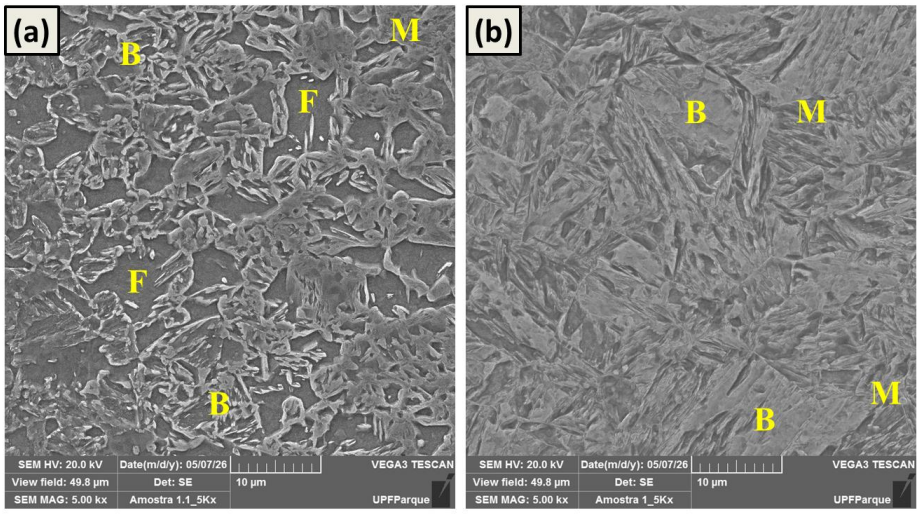


Fig. 11 Microstructure of experimental condition EC1 obtained by SEM for the regions of (a) heat affected zone and (b) cast zone



Thus, although local variations in the proportion of constituents could be observed among conditions EC1, EC2, EC3, and EC4, the overall microstructural trend remained similar. The regions closest to the cut edge,

directly exposed to the laser beam, exhibited a more refined microstructure and a higher fraction of hard constituents, whereas ferrite became more prevalent in the heat affected zone and the base material.

Fig. 12 Microstructure of experimental condition EC2 obtained by SEM for the regions of (a) heat affected zone and (b) cast zone

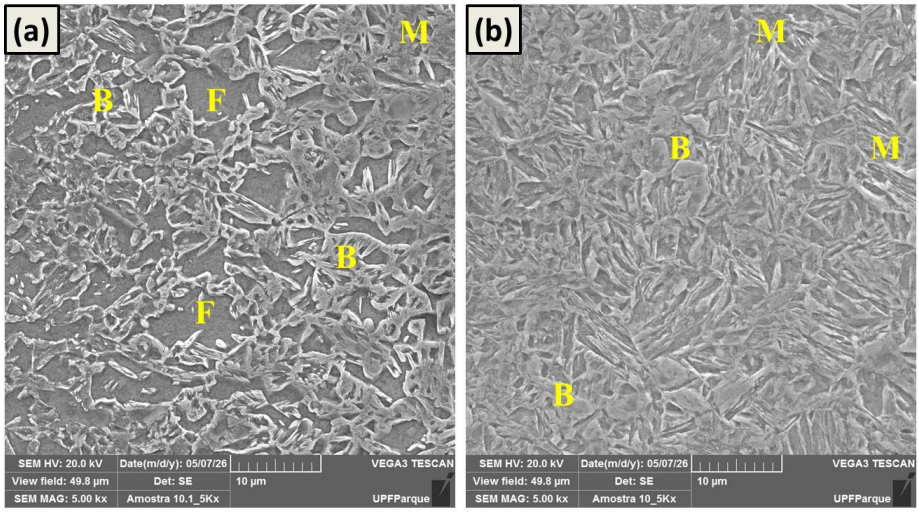
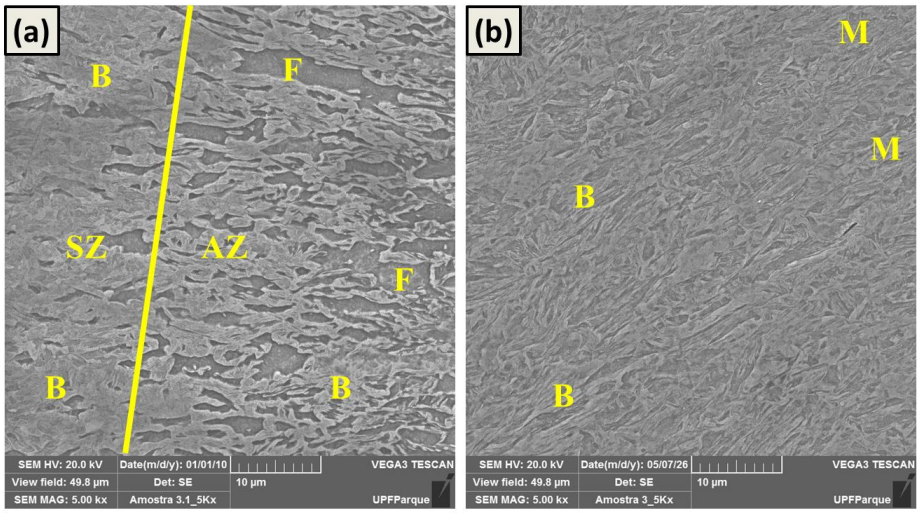


Fig. 13 Microstructure of experimental condition EC3 obtained by SEM for the regions of (a) heat affected zone and (b) cast zone

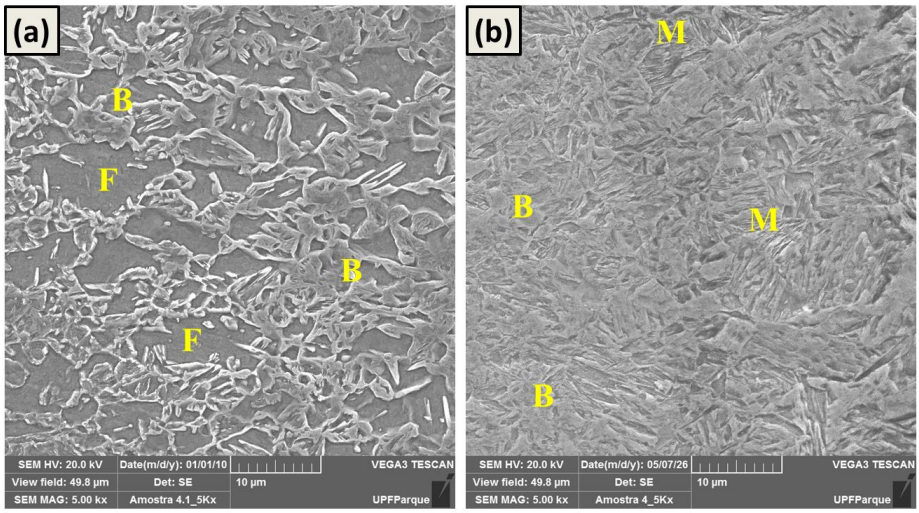


This behavior is corroborated by the microhardness analysis of these regions. From Fig. 15, a correlation can be observed between the lower fraction of softer constituents and the increase in microhardness within the cast zone. In contrast, the heat affected zone and the base material, due to their more similar microstructures, exhibited closer microhardness values. Therefore, the observed microstructural differences support the microhardness variation discussed in the following section.

As a result of the thermal exposure associated with laser cutting, microstructural variations are induced in the cut region, particularly as a function of energy density, the employed assist gas, and the elevated heating and cooling rates. In the cast zone, the material is heated until melting and subsequently subjected to rapid solidification, favoring microstructural refinement and the formation of bainite and constituents with

morphology compatible with martensite. This behavior contributes to the increase in hardness within this region, although thermal exposure may also promote localized tempering phenomena and grain growth in the heat affected zone. Similar behavior was observed in 22MnB5 steel, in which laser cutting may promote complete transformation of the ferritic-pearlitic microstructure into martensite, resulting in a significant increase in hardness (26).

Fig. 14 Microstructure of experimental condition EC4 obtained by SEM for the regions of (a) heat affected zone and (b) cast zone



3.3. Vickers Microhardness

The cast regions, i.e., those that underwent melting followed by solidification and are located closest to the cut edge, exhibited higher microhardness than the base material, regardless of the cutting parameters analyzed, as shown in Fig. 15. This behavior is associated with the formation of a microstructure predominantly composed of bainite and constituents with morphology compatible with martensite, as discussed in the previous section.

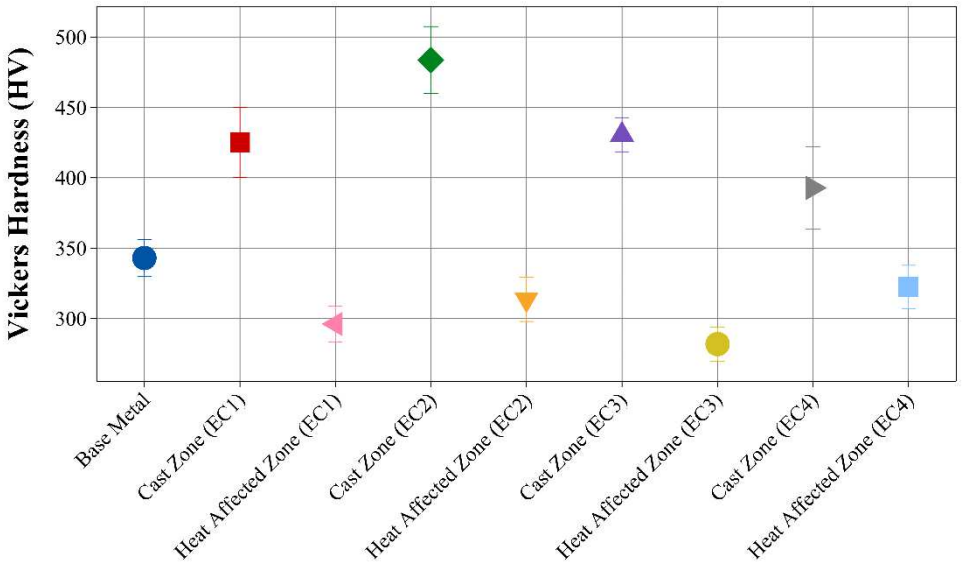
On the other hand, the heat affected zone, located between the cast zone and the base material, exhibited lower microhardness than the base material and, consequently, than the cast zone. This behavior is associated with tempering and microstructural recovery effects promoted by the thermal cycle of laser cutting, which reduce the microhardness of this region (23-25).

Thus, the microhardness behavior observed in the regions modified by laser cutting is directly related to changes in phase balance and microstructural morphology. In the cast zone, the higher presence of bainite and constituents compatible with martensite contributes to the increase in microhardness. In contrast, the heat affected zone exhibits lower microhardness due to the action of the thermal cycle on the pre-existing constituents and the higher relative presence of softer constituents. Edge hardening, associated with the higher fraction of hard phases, has also been observed in studies involving laser cutting of S355NC steel and AISI 304 stainless steel (20, 27).

Microhardness is predominantly dependent on the material microstructure; therefore, operational parameters capable of altering microstructural formation also directly influence the microhardness of the regions

modified by cutting. In steels subjected to laser cutting, laser power plays a relevant role, since higher heat inputs tend to alter both the extent of the affected region and the resulting microstructural transformations (7-8). However, this behavior is not uniform for all regions, as the increase in thermal energy may also favor a reduction in the local cooling rate, grain growth, and changes in the balance between bainite and constituents compatible with martensite.

Fig. 15 Average values of Vickers microhardness



The ANOVA results for the heat affected zone and the cast zone demonstrated that microhardness was strongly influenced by the interaction between laser power and assist gas. In the heat affected zone, all evaluated factors were statistically significant, with the interaction between power and assist gas being the main source of variation (40.97%), followed by laser power (31.53%) and assist gas (16.43%). In turn, for the cast zone, laser power alone did not present a statistically significant effect ($p = 0.332$), whereas the assist gas (24.88%) and, particularly, the interaction between laser power and assist gas (53.65%) were significant. This behavior indicates that the microhardness of the regions modified by cutting should not be interpreted solely based on the isolated effects of the parameters, but rather considering the combination of heat input, cutting atmosphere, and cooling conditions.

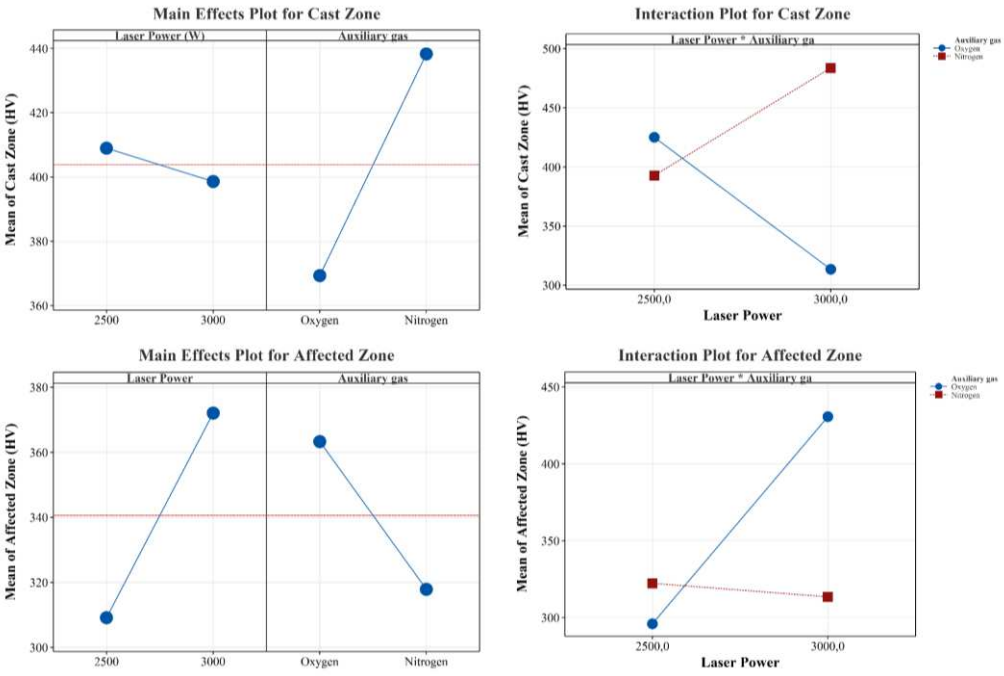
In this context, the main effect plots presented in Fig. 16 should be interpreted together with the ANOVA results. For the cast zone, although the plot indicates a reduction in average microhardness values with increasing laser power, this isolated effect was not statistically significant and should therefore be interpreted with caution. In contrast, in the heat affected zone, increasing the laser power from 2500 W to 3000 W promoted an increase in average microhardness, a behavior supported by the statistical significance observed in the ANOVA.

Additionally, the influence of the assist gases manifested itself differently between the analyzed regions. In the cast zone, the use of nitrogen resulted in higher average microhardness values than those obtained with oxygen, whereas the opposite behavior was observed in the heat affected zone. Furthermore, the interaction plots presented in Fig. 16 reveal, for both studied regions, the existence of interaction between the analyzed

variables, a behavior also confirmed by the ANOVA results. This response demonstrates that microhardness is governed by the combination of laser power and the condition associated with the assist gas, rather than by the isolated action of each factor.

It should be considered that assist gas type, gas pressure, and cutting speed varied simultaneously between the oxygen and nitrogen conditions. Therefore, the microhardness differences attributed to the assist gas should be interpreted as the result of the combined influence of these parameters. Even considering this limitation, the results indicate that the nitrogen-associated condition favored higher microhardness values in the cast zone, whereas the oxygen-associated condition resulted in higher values in the heat affected zone. This behavior occurs because, whereas oxygen intensifies exothermic reactions during cutting, nitrogen promotes cooling of the cut surface (6, 20).

Fig. 16 Main effect and interaction plots for the Vickers microhardness of the cast zone and the heat affected zone



3.4. Surface Roughness

The surface roughness parameters, both Ra and Rz, were higher at the cut exit than at the cut entry for all experimental conditions, with variations ranging from 184.01% to 430.45%, as shown in Figs. 17 and 18. This behavior demonstrates that the surface quality of the cut edge is not uniform throughout the sheet thickness, with the exit region being more susceptible to the formation of surface irregularities. This tendency is corroborated by the analysis of Fig. 20, in which a greater presence of cutting marks, striations, and burrs can be observed in the exit region. Furthermore, the increase in roughness with increasing distance from the cut entry surface has also been reported in the literature. For example, in commercially pure titanium sheets, the Ra value increases as the distance from the cut entry increases, with variations ranging between 180% and 280% (28).

The ANOVA results for Ra and Rz confirm that the measurement position was the dominant factor in the variation of surface roughness. For Ra, the position accounted for 77.94% of the total variation, whereas for

Rz its contribution was 66.77%, indicating that the difference between the cut entry and exit exerted a much greater influence than the isolated parameters of laser power and assist gas. For Ra, laser power presented a significant effect, although with a low contribution of 2.33%, whereas the assist gas alone was not statistically significant. For Rz, both laser power and assist gas were significant, but likewise with low contributions of 3.27% and 3.45%, respectively.

Fig. 17 Average Ra values at the cut entry and cut exit for different experimental conditions

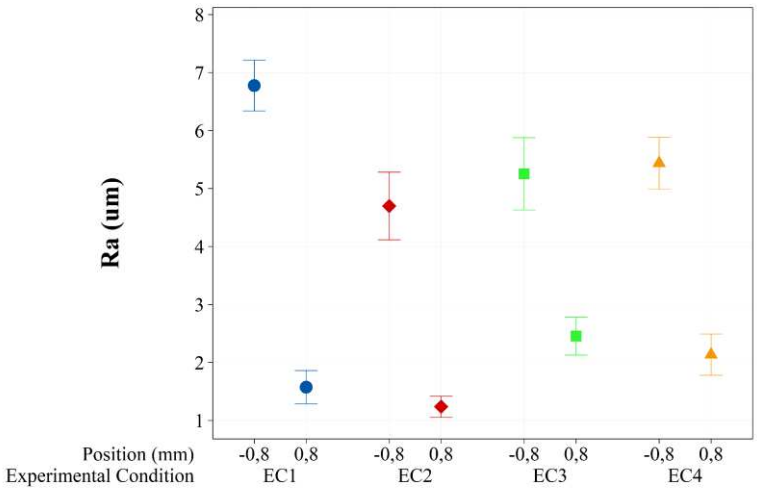
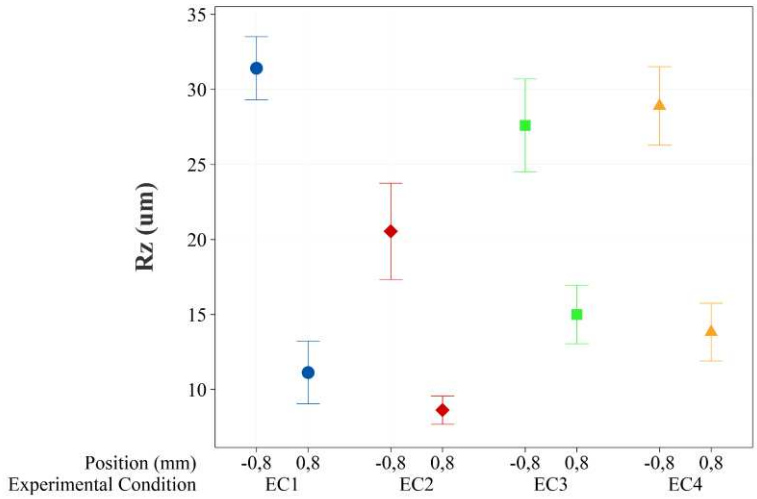


Fig. 18 Average Rz values at the cut entry and cut exit for different experimental conditions

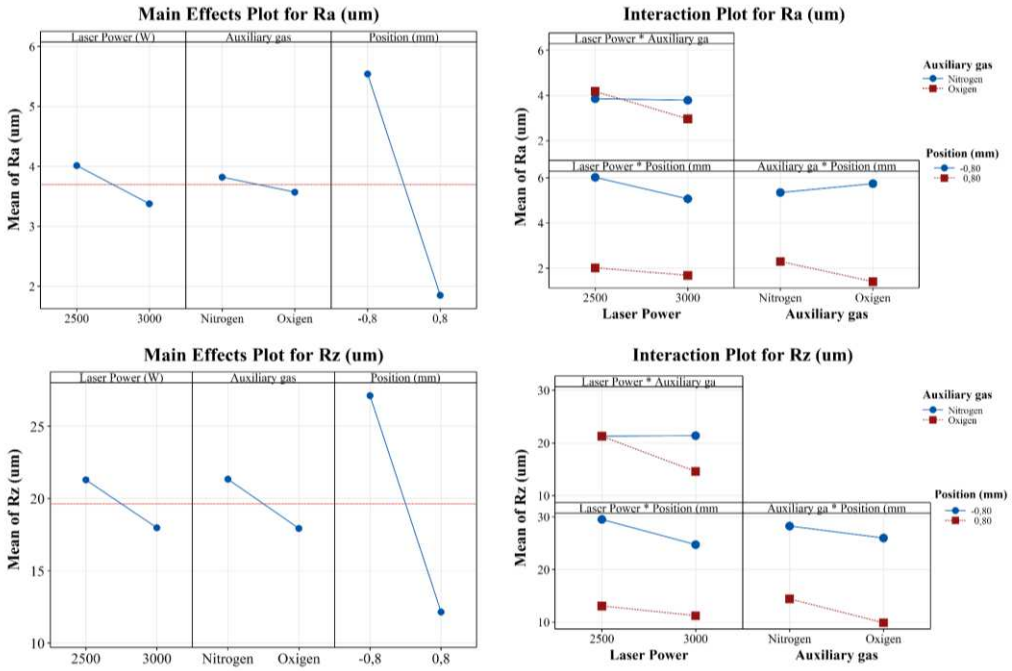


Thus, the main effect and interaction plots presented in Fig. 19 should be interpreted as a visual complement to the ANOVA results. Although increasing laser power reduced the average roughness values within the investigated parameter range, this effect was secondary compared with the measurement position. Furthermore, the significant interactions observed, especially for Ra and for the triple interaction in Rz, indicate that the roughness response depends on the combination of laser power, assist gas, and measurement position, rather than on the isolated action of each parameter.

The increase in roughness with cutting depth can be attributed to the combination of thermal, dynamic, and optical factors inherent to the process, including the reduction in effective beam intensity, progressive

defocusing throughout the material thickness, and changes in molten material flow. These factors compromise material removal and favor the formation of thicker, inclined, or irregular striations in the cut exit region (7). Furthermore, instabilities at the cutting front, such as hump formation and interrupted striations, alter local energy absorption and impair surface finish uniformity, potentially involving intense metal vaporization events (9, 29).

Fig. 19 Main effect and interaction plots for Ra and Rz

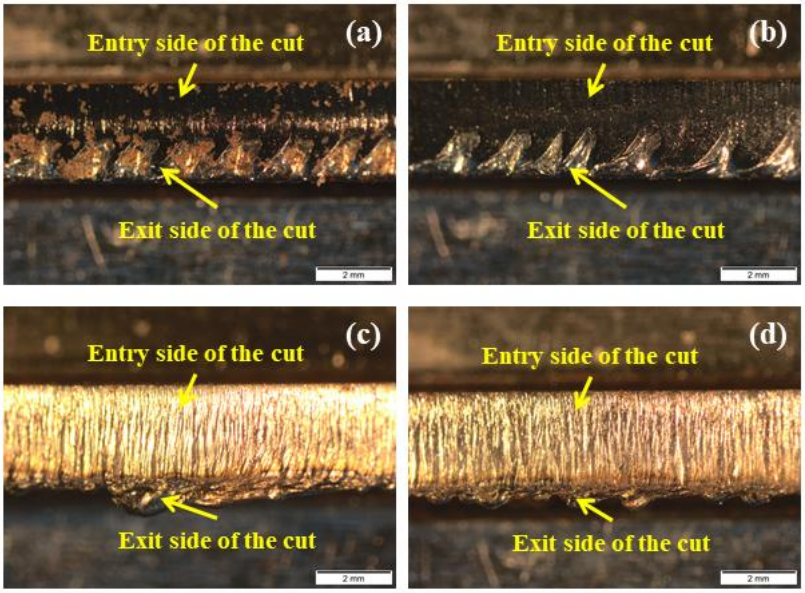


The analysis of the cut surfaces presented in Fig. 20 reinforces the results obtained for Ra and Rz, especially regarding the greater surface degradation at the cut exit. The more pronounced presence of cutting marks and burrs in this region is consistent with the dominant contribution of the measurement position observed in the ANOVA analysis. Therefore, the position along the sheet thickness should be considered the main factor associated with the surface integrity of the cut edge in this study.

The laser cutting process depends on the high energy density concentrated in a localized region, promoting rapid heating, melting, vaporization, and expulsion of molten material. Within the investigated parameter range, higher laser power values resulted in lower average roughness values, although this effect presented a relatively low contribution when compared with the measurement position. Similar behavior was observed in the laser cutting of Strenx 900 steel, in which the Taguchi methodology indicated improved surface finish under the higher power condition (30).

Additionally, the analysis of S700MC and S890Q steels reinforces that surface roughness, together with slag adhesion, constitutes one of the quality indicators most sensitive to thermal cutting parameters. Similarly to what was observed for Strenx 900 steel, the authors confirmed that laser beam power and cutting speed are relevant factors in defining the quality of the cut edge (31).

Fig. 20 Surface finish of the cut edges for the experimental conditions: (a) EC1; (b) EC2; (c) EC3; and (d) EC4



3.5. Fatigue Resistance

The retention of the regions modified by laser cutting substantially reduced the fatigue life of the specimens compared with the machined condition (OG), in which the cast zone and the heat affected zone were removed. For the loading condition corresponding to 70% of the tensile strength of the material, the reduction in the number of cycles sustained ranged from 81% to 83%. Similar behavior was observed at the lower loading level, corresponding to 50% of the tensile strength, for which the reduction ranged from 71% to 75% for most conditions. However, condition EC2 exhibited exceptional behavior when subjected to a stress level of 539 MPa, achieving fatigue life significantly higher than the other conditions, as shown in Fig. 21.

The exceptional fatigue resistance exhibited by EC2 under loading corresponding to 50% of the tensile strength may be associated with the lower geometric severity of the cut edge and a microstructural condition more favorable to crack nucleation resistance. Tukey's test indicated that EC2 was the only condition statistically distinct for Rz, presenting the lowest average value among all evaluated conditions. This result is particularly relevant because Rz is more sensitive to extreme peaks and valleys than Ra, providing a better representation of the severity of surface notches that act as fatigue crack nucleation sites (6). Although Ra did not statistically differentiate the experimental conditions, EC2 also exhibited the lowest absolute average value, reinforcing the hypothesis of lower local surface severity (27, 32-33). This behavior is consistent with the fractographs presented in Figs. 22 and 23, in which crack nucleation occurred predominantly at the cut exit, a region more susceptible to the presence of striations, burrs, and surface irregularities.

However, this benefit was not observed under loading corresponding to 70% of the tensile strength, indicating that the superior performance of EC2 was primarily associated with delayed crack nucleation, which is the most critical stage under lower stress regimes (5, 17). Under more severe loading conditions, the intensity of local stresses generated by surface defects tends to outweigh the beneficial effects of lower roughness and the more favorable microstructural condition of the cut edge, resulting in similar fatigue lives among the evaluated conditions. This behavior is consistent with that observed in ultra-high-strength steels such as S960MC, in which

higher mechanical strength increases sensitivity to cutting defects and reduces tolerance to surface discontinuities (19). In this context, it can be observed that, under high loading regimes, the geometric defects inherent to the cutting process exert a more pronounced influence on fatigue performance than the Ra and Rz roughness values considered individually (32-33).

Fig. 21 Stress versus number of cycles to failure

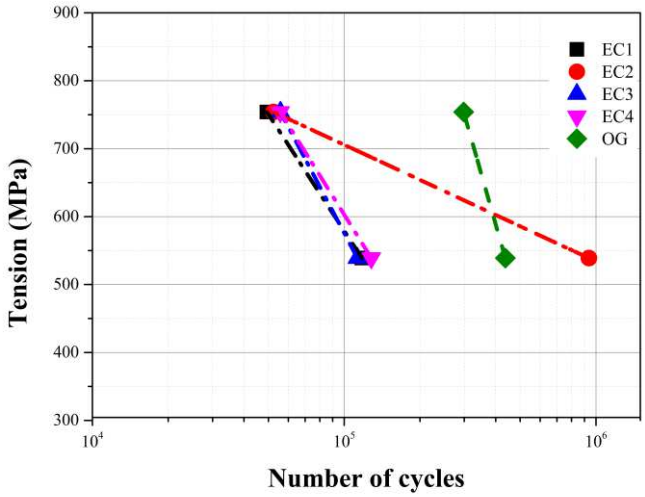


Fig. 22 Fractographs of a fatigue-fractured specimen under loading corresponding to 50% of the tensile strength of the material in its original condition, with magnifications of (a) 35×, (b) 1000×, (c) 2000×, and (d) 5000×

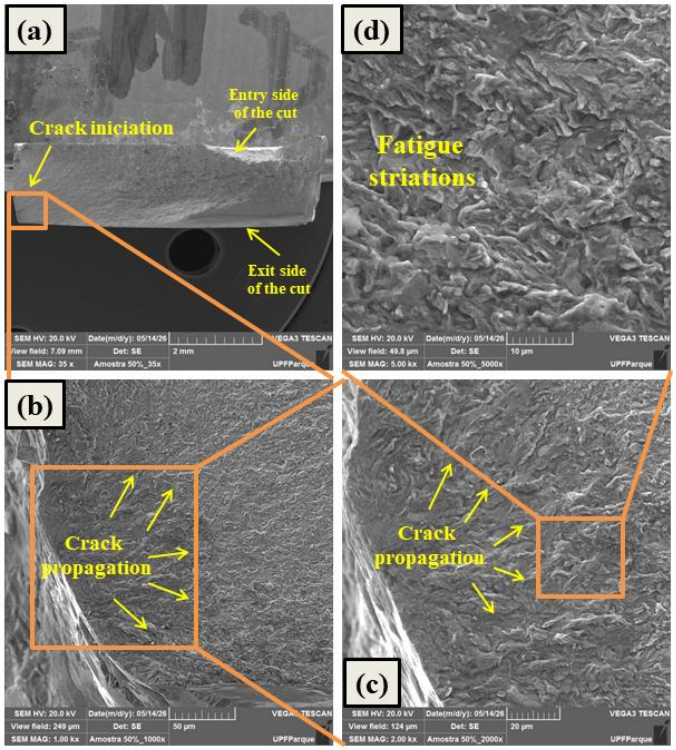
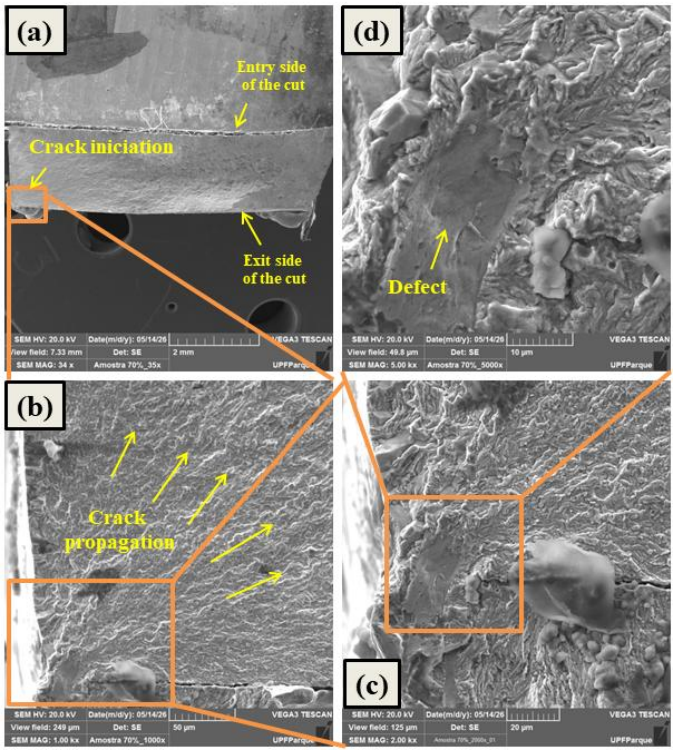


Fig. 23 Fractographs of a fatigue-fractured specimen under loading corresponding to 70% of the tensile strength of the material in its original condition, with magnifications of (a) 35×, (b) 1000×, (c) 2000×, and (d) 5000×



Overall, the literature indicates that laser cutting can reduce the fatigue life of high-strength steels due to the combined effects of surface integrity degradation, the presence of the HAZ, microstructural modifications, and the formation of tensile residual stresses. In S700MC steel, for example, thermal cycles reduced the fatigue strength from 500 MPa to 335 MPa, with residual stresses accounting for 69% of this reduction (3). In particular, tensile residual stresses are known to accelerate crack nucleation and, together with grain growth in the HAZ, can significantly degrade the cyclic properties of the material (22).

Furthermore, irregularities such as striations, waviness, burrs, and pronounced peaks and valleys act as stress concentrators, promoting crack nucleation in components subjected to cyclic loading (16, 18-19, 21, 34). The presence of burrs is recognized as one of the most critical discontinuities in ultra-high-strength steels cut by fusion-based processes, serving as a preferential site for crack nucleation and propagation (32).

On the other hand, the adoption of optimized processing parameters and post-processing treatments can improve fatigue performance by reducing the geometric severity of the cut edge. This effect was observed in S690Q steel, whose fatigue strength increased from 179 MPa to 209 MPa after improvement of the edge geometry, and in joints subjected to laser dressing, for which the fatigue class increased from 140 MPa to 166 MPa (5, 27).

Additionally, the mechanical removal of hardened burrs can increase fatigue life by 63% in S690 steel and by an impressive 147% in S1100 steel (32). Even in mechanical processes such as punching, grinding the cut edges to remove the work-hardened and rough layer results in an increase of 11% to 15% in the supported stress amplitude (21). The choice of assist gas also plays a crucial role; in S1100 steel, reactive oxygen cutting produced more uniform edges and superior fatigue performance compared with fusion cutting using nitrogen, which was more prone to the formation of microdefects and porosity (32).

4. CONCLUSIONS

The present study investigated the influence of laser cutting conditions on the surface integrity, microstructure, microhardness, and fatigue performance of Strenx 700CR steel. The main conclusions are summarized as follows:

- Thermally Modified Zones and Parameter Influence: Laser cutting produced a cast zone (CZ) and a heat affected zone (HAZ), both exhibiting greater extent near the beam entry region. The areas of these regions increased when laser power was raised from 2500 W to 3000 W and were larger under oxygen-associated conditions. The condition associated with the assist gas was the dominant factor, contributing 63.15% and 79.40% to the variation of the HAZ and CZ areas, respectively, followed by laser power, with contributions of 12.92% and 18.12%.
- Microstructure and Microhardness Gradient: The CZ exhibited a lower ferrite fraction and a higher presence of bainite and constituents compatible with martensite, resulting in microhardness values higher than those of the base material. In contrast, the HAZ exhibited softening associated with tempering and microstructural recovery effects. Microhardness was primarily governed by the interaction between laser power and the condition associated with the assist gas, contributing 40.97% of the variation in the HAZ and 53.65% in the CZ.
- Surface Integrity: Surface roughness was higher at the cut exit than at the cut entry for all experimental conditions, with increases ranging from 184.01% to 430.45%. The measurement position was the predominant factor, accounting for 77.94% of the variation in Ra and 66.77% of the variation in Rz, indicating that the cut exit is the most critical region regarding the presence of striations, burrs, and surface irregularities.
- Fatigue Performance and Failure Mechanisms: The retention of the regions modified by laser cutting reduced fatigue life compared with the machined condition, with reductions ranging from 81% to 83% under loading corresponding to 70% of the tensile strength and from 71% to 75% under loading corresponding to 50% of the tensile strength for most conditions. Condition EC2 exhibited exceptional performance under 539 MPa, possibly due to the lower geometric severity of the cut edge, associated with its lower Rz value. Fractographic analyses revealed that crack nucleation occurred predominantly at the cut exit, confirming the role of surface irregularities as stress concentrators.

Acknowledgements: The authors would like to thank Stara S.A., a company in the agricultural machinery sector, for the support provided through the supply of materials and assistance with the processes involved in this study. The authors also thank the University of Passo Fundo, especially the Materials Laboratory, for the technical support and infrastructure made available for the experimental analyses.

Author Contributions: João Vitor Miszewski established the laser cutting procedure, contributed to the manuscript writing, and conducted the statistical analysis of the data. William Haupt proposed the study methodology, performed the experimental laboratory analyses, and assisted in writing the manuscript Diogo Teixeira assisted in writing and reviewing the manuscript, as well as in preparing drawings and tables. Cleiton Gnich contributed to writing the manuscript and performed the statistical analysis of the microhardness data. Matheus Giongo Pavan reviewed the final version of the manuscript and assisted in the analysis of the

fatigue test results. Finally, André Amaral dos Santos contributed to obtaining the roughness data and to their statistical analysis.

Funding: Stara S.A. provided the materials used in this study, while the experimental and metallurgical analyses were performed in the laboratories of the University of Passo Fundo (UPF). No additional financial support was received for the development of this research beyond that previously declared.

Data Availability: The datasets generated and analyzed during the current study are available from the corresponding author upon reasonable request.

DECLARATIONS

Ethics Approval: All authors of the manuscript entitled "Microstructural Evolution, Surface Integrity and Fatigue Resistance of Laser-Cut Strenx 700CR Steel" declare that the work contains original research results and has neither been published nor simultaneously submitted to another journal up to the present moment. The applicable ethical principles were strictly followed throughout the development of the research. All authors agree with the submission of the manuscript to the journal Lasers in Manufacturing and Materials Processing.

Conflict of Interest: The authors declare that there are no conflicts of interest.

REFERENCES

1. Reinhardt, L., Vogelmann, A., Krüger, S.: Emerging trends in advanced metallic materials for lightweight engineering applications. Int. J. Mater. Sci. **7**, 49–53 (2026). https://doi.org/10.22271/27078221.2026.v7.i1a.105
2. Rukavina, M. J., Skejić, D., Kralj, A., Ščapec, T., Milovanović, B.: Development of lightweight steel framed construction systems for nearly-zero energy buildings. Buildings **12**, 929 (2022). https://doi.org/10.3390/buildings12070929
3. Bukovská, Š., Moravec, J., Solfronk, P., Pekárek, M.: Assessment of the effect of residual stresses arising in the HAZ of welds on the fatigue life of S700MC steel. Metals **12**, 1890 (2022). https://doi.org/10.3390/met12111890
4. Eichler, S., von Arnim, M., Brätz, O., Hildebrand, J., Gericke, A., Bergmann, J.P., Kuhlmann, U., Henkel, K.-M.: Heat management and tensile strength of 3 mm mixed and matched connections of butt joints of S355J2+N, S460MC and S700MC. ce/papers **6**, 1476–1482 (2023). https://doi.org/10.1002/cepa.2265
5. Mičian, M., Frátrik, M., Moravec, J., Jambor, M., Solfronk, P., Šulák, I.: Enhancement of fatigue performance of thin HSLA steel laser-welded butt joints. Welding in the World (2025). https://doi.org/10.1007/s40194-025-02193-1
6. Sales-Contini, R.C.M., Amaral, I., Lucas, R.R., Pinto, A.M.G., Campilho, R.D.S.G., Magalhães, L.L., da Silva, F.J.G.: Optimizing laser cutting parameters for enhanced surface quality in mild and stainless steel: an experimental study. Engineering Reports **7**, 7 (2025). https://doi.org/10.1002/eng2.70283
7. Alsaadawy, M., Dewidar, M., Said, A., Maher, I., Shehabeldeen, T.A.: A comprehensive review of studying the influence of laser cutting parameters on surface and kerf quality of metals. Int. J. Adv. Manuf. Technol. **130**, 1039–1074 (2023). https://doi.org/10.1007/s00170-023-12768-1
8. Safari, M., Abtahi, S.M., Joudaki, J.: Experimental modeling, statistical analysis, and optimization of the laser-cutting process of Hardox 400 steel. Materials **17**, 2798 (2024). https://doi.org/10.3390/ma17122798
9. Sawannia, M., Powell, J., Borkmann, M., Hagenlocher, C., Graf, T.: Laser cutting: experimental measurement of fluctuations in cut front temperature and morphology. Lasers Manuf. Mater. Process. **13**, 45–62 (2026). https://doi.org/10.1007/s40516-025-00324-6
10. Nisar, S.: Optimization of laser beam geometry for controlling thermal stresses in CO_2 laser glass cutting. Lasers Manuf. Mater. Process. **12**, 298–317 (2025). https://doi.org/10.1007/s40516-025-00289-6

11. Chen, J., Shi, Z., Luo, X., Chai, F., Pan, T., Feng, G., Yang, C.: Micro-alloying effects on microstructure and weldability of high-strength low-alloy steel: A review. Materials **18**, 1036 (2025). https://doi.org/10.3390/ma18051036
12. Tian, Z., Tian, Y., Sun, D., Feng, X., Yang, Z., Zhang, F.: A review on phase transformation mechanisms and process control for strengthening and toughening of V-microalloyed bainitic steels. J. Mater. Res. Technol. **41**, 2883–2903 (2026). https://doi.org/10.1016/j.jmrt.2026.01.157
13. Liao, Z., la Monaca, A., Murray, J., Speidel, A., Ushmaev, D., Clare, A., Axinte, D., M'Saoubi, R.: Surface integrity in metal machining – Part I: Fundamentals of surface characteristics and formation mechanisms. International Journal of Machine Tools and Manufacture **162**, 103687 (2021). https://doi.org/10.1016/j.ijmachtools.2020.103687
14. Pimenov, D. Y., Kiran, M., Khanna, N., Pintaude, G., Vasco, M. C., da Silva, L. R. R., Giasin, K.: Review of improvement of machinability and surface integrity in machining on aluminum alloys. Int. J. Adv. Manuf. Technol. **129**, 4743–4779 (2023). https://doi.org/10.1007/s00170-023-12630-4
15. Lopes, M. O., Petring, D., Stoyanov, S., Gillner, A.: Control of melt dynamics in laser cutting based on a resonant nozzle cavity. Journal of Manufacturing Processes **105**, 399–406 (2023). https://doi.org/10.1016/j.jmapro.2023.09.051
16. Qutaba, S., Asmelash, M., Saptaji, K., Azhari, A.: A review on peening processes and its effect on surfaces. Int. J. Adv. Manuf. Technol. **120**, 4233–4270 (2022). https://doi.org/10.1007/s00170-022-08882-8
17. Song, Y., Zhang, C., Cheng, Z., Chen, Y. A., Wang, S. Z., Zhu, D. X., Wu, H. H.: Fatigue properties of microalloyed steels: a review. Journal of Iron and Steel Research International **32**, 2213–2231 (2025). https://doi.org/10.1007/s42243-024-01284-x
18. Zhang, Y., Wang, C., Xu, W., Zhang, X., Ren, K., Wang, S., Hua, Q.: Laser cutting of titanium alloy plates: a review of processing, microstructure, and mechanical properties. Metals **14**, 1152 (2024). https://doi.org/10.3390/met14101152
19. Yılmaz, O., van Hoecke, D.: Hole-making and cutting effects on fatigue performance of ultra high strength steels. Procedia Structural Integrity **57**, 420–427 (2024). https://doi.org/10.1016/j.prostr.2024.03.045
20. Selech, J., Burzyński, G., Tibebe, D., Ulbrich, D., Banas, P.: Influence of laser cutting parameters on the microhardness, roughness, and microstructure of AISI 304, S355J2, and $AlMg_3$ alloys. Materials **19**, 240 (2026). https://doi.org/10.3390/ma19020240
21. Chmelko, V., Košèo, M.: Influence of manufacturing processes to the fatigue strength of thin steel plates. Procedia Structural Integrity **76**, 131–137 (2025). https://doi.org/10.1016/j.prostr.2025.12.296
22. Trško, L., Lago, J., Jambor, M., Nový, F., Bokůvka, O., Florková, Z.: Microstructure and residual stress analysis of Strenx 700 MC welded joint. Production Engineering Archives **26**, 41–44 (2020). http://dx.doi.org/10.30657/pea.2020.26.09
23. Ilin, I. A., Krasnoperova, A. A., Sirotkin, E. A.: Effect Study of Thermal Cutting Methods on the Edge's Microstructure of High-Strength Steel Grade S700MC. Materials Science Forum **946**, 928–933 (2019). https://doi.org/10.4028/www.scientific.net/MSF.946.928
24. Kim, K., Kang, N., Kang, M., Kim, C.: Assessment of heat-affected zone softening of hot-press-formed steel over 2.0 GPa tensile strength with bead-on-plate laser welding. Applied Sciences **11**, 5774 (2021). https://doi.org/10.3390/app11135774
25. Afkhami, S., Javaheri, V., Amraei, M., Skriko, T., Piili, H., Zhao, X.-L., Björk, T.: Thermomechanical simulation of the heat-affected zones in welded ultra-high strength steels: Microstructure and mechanical properties. Materials & Design **213**, 110336 (2022). https://doi.org/10.1016/j.matdes.2021.110336
26. Tahir, A. F. M., Rashid, A. R., Sariff, N. E., Rahim, E. A.: CO2 laser cutting performance on ultra high strength steel (UHSS). Lasers Manuf. Mater. Process. **7**, 15–37 (2020). https://doi.org/10.1007/s40516-019-00104-z
27. Diekhoff, P., Hensel, J., Nitschke-Pagel, T., Dilger, K.: Investigation on fatigue strength of cut edges produced by various cutting methods for high-strength steels. Welding in the World **64**, 545–561 (2020). https://doi.org/10.1007/s40194-019-00851-x
28. Boujelbene, M., El-Aoud, B., Bayraktar, E., Elbadawi, I., Chaudhry, I., Khaliq, A., Ayyaz, A., Elleuch, Z.: Effect of cutting conditions on surface roughness of machined parts in CO2 laser cutting of pure titanium. Materials Today: Proceedings **44**, 2080–2086 (2021). https://doi.org/10.1016/j.matpr.2020.12.179
29. Bocksrocker, O., Berger, P., Kessler, S., Hesse, T., Rominger, V., Graf, T.: Local vaporization at the cut front at high laser cutting speeds. Lasers Manuf. Mater. Process. **7**, 190–206 (2020). https://doi.org/10.1007/s40516-020-00113-3
30. Muralidharan, K., Kamala, S. P., Alankrutha, D., Prakash, K. B., Subbiah, R., Marichamy, S.: Parametric analysis and performance of laser cutting on Strenx steel. Materials Today: Proceedings (2020). https://doi.org/10.1016/j.matpr.2020.10.573

31. Klimpel, A., Cholewa, W., Bannister, A., Łuksa, K., Przystałka, P., Rogala, T., Skupień, D., Cicero, S., Martín-Meizoso, A.: Experimental investigations of the influence of laser beam and plasma arc cutting parameters on edge quality of high-strength low-alloy (HSLA) strips and plates. Int. J. Adv. Manuf. Technol. **92**, 699–713 (2017). https://doi.org/10.1007/s00170-017-0119-2
32. Lipiäinen, K., Ahola, A., Skriko, T., Björk, T.: Fatigue strength characterization of high and ultra-high-strength steel cut edges. Engineering Structures **228**, 111544 (2021). https://doi.org/10.1016/j.engstruct.2020.111544
33. Rowiński, S.: Effect of steel-cutting technology on fatigue strength of steel structures: Tests and analyses. Materials **14**, 6097 (2021). https://doi.org/10.3390/ma14206097
34. Kharche, N. A., Sulakhe, V. N., Baviskar, P. R., Kaware, K.: An extensive review of the effects of laser cutting parameters on metal surface and kerf quality. Res. Eng. Struct. Mater. **12**, 467–485 (2026). http://dx.doi.org/10.17515/resm2025-953ma0608rv